Observation of paramagnetic spin-degeneracy lifting in $EuZn_2Sb_2$

Milo X. Sprague,[1] Sabin Regmi,[1,2] Barun Ghosh,[3,6] Anup Pradhan Sakhya,[1] Mazharul Islam Mondal,[1] Iftakhar Bin Elius,[1] Nathan Valadez,[1] Bahadur Singh,[4] Tetiana Romanova,[5] Dariusz Kaczorowski,[5] Arun Bansil,[3,6] and Madhab Neupane[1,*]

[1]*Department of Physics, University of Central Florida, Orlando, Florida 32816, USA*
[2]*Center for Quantum Actinide Science and Technology, Idaho National Laboratory, Idaho Falls, Idaho 83415, USA*
[3]*Department of Physics, Northeastern University, Boston, Massachusetts 02115, USA*
[4]*Department of Condensed Matter Physics and Materials Science, Tata Institute of Fundamental Research, Mumbai 400005, India*
[5]*Institute of Low Temperature and Structure Research, Polish Academy of Sciences, ulitsa Okólna 2, PL-50-422 Wrocław, Poland*
[6]*Quantum Materials and Sensing Institute, Northeastern University, Burlington, Massachusetts 01803, USA*

(Received 25 May 2023; revised 9 May 2024; accepted 24 June 2024; published 16 July 2024)

Taken together, time-reversal and spatial inversion symmetries impose a twofold spin degeneracy of the electronic states in crystals. In centrosymmetric materials, this degeneracy can be lifted by introducing magnetism, either via an externally applied field or through internal magnetization. However, a correlated alignment of spins, even in the paramagnetic phase, can lift the spin degeneracy of electronic states. Here, we report an in-depth study of the electronic band structure of the Eu-ternary pnictide $EuZn_2Sb_2$ through a combination of high-resolution angle-resolved photoemission spectroscopy measurements and first-principles calculations. An analysis of the photoemission line shapes over a range of incident photon energies and sample temperatures is shown to reveal the presence of band spin-degeneracy lifting in the paramagnetic phase. Our angle-resolved photoemission spectroscopy results are in good agreement with theoretical ferromagnetic-phase calculations, which indicates the importance of ferromagnetic fluctuations in the system. Through our calculations, we predict that spin-polarized bands in $EuZn_2Sb_2$ generate a single pair of Weyl nodes. Our observation of band splitting in $EuZn_2Sb_2$ provides a key step toward realizing time-reversal symmetry breaking physics in the absence of long-range magnetic order.

DOI: 10.1103/PhysRevB.110.045130

I. INTRODUCTION

Symmetry has become a significant organizing principle in modern condensed matter physics. Symmetries enforce protected degeneracies along high-symmetry directions in the Brillouin zone (BZ), which can dramatically simplify the analysis of electronic band structures [1]. Consideration of symmetries has also led to efficient classification schemes for topologically protected states [2]. Topological insulators provided the first example of a three-dimensional (3D) symmetry protected topological material [3–6]. Time-reversal symmetry (TRS) and bulk inversion symmetry (IS) were shown to protect spin-orbit induced band inversions and twofold band crossings between spin-polarized Dirac surface states pinned to the TRS points of the BZ [3,7–9]. These symmetries can also protect the fourfold degenerate band crossings in bulk-3D Dirac semimetals [10–13]. The breaking of TRS in topological insulators and Dirac semimetals can lead to new topological phases such as the magnetic topological insulators [14] and the Weyl semimetals [13,15].

Effects of TRS breaking are usually explored in the context of materials with net magnetization. However, short-ranged correlated spin alignments can provide another mechanism for lifting the Kramers degeneracy [16]. Given large enough correlation lengths and times, it can be anticipated that similar TRS-breaking physics may be observed in materials [17]. Zintl-phase EuX_2Pn_2, with transition metal X and pnictogen Pn, most notably $EuCd_2As_2$ and $EuZn_2As_2$, have been recognized for supporting nonlinear anomalous Hall and anomalous Nernst effects [18,19], electron spin resonance (ESR) [17,20,21], muon spin relaxation [17], and resonant elastic x-ray scattering [22] responses that are consistent with the formation of slowly fluctuating ferromagnetic domains in the paramagnetic phase. These results indicate the possibility of producing spin-polarized electronic states in paramagnetic samples, where both the global TRS and IS are preserved. The low-energy physics of EuX_2Pn_2 systems are dominated by the interplay of transition-metal-s conduction bands and pnictide-p valence bands near the Γ point [23]. The precise energetics are strongly dependent on spin-orbit coupling strength and details of the resulting magnetic ordering. This interplay of magnetism and spin-orbit coupling stabilizes a variety of magnetic and nonmagnetic topological phases [17,23–33].

The recent interest in $EuZn_2As_2$ and $EuCd_2As_2$ naturally motivates continuing work on $EuZn_2Sb_2$ due to its intermediate spin-orbit coupling strength. $EuZn_2Sb_2$ has been observed to produce ESR line shapes consistent with slow ferromagnetic correlations ranging from the antiferromagnetic (AFM) transition temperature ($T_N = 13$ K) to over 100 K [20]. Given the connection between magnetic fluctuations and electronic structure established both theoretically [16] and through recent experiments [17–22], the potential

*Contact author: madhab.neupane@ucf.edu

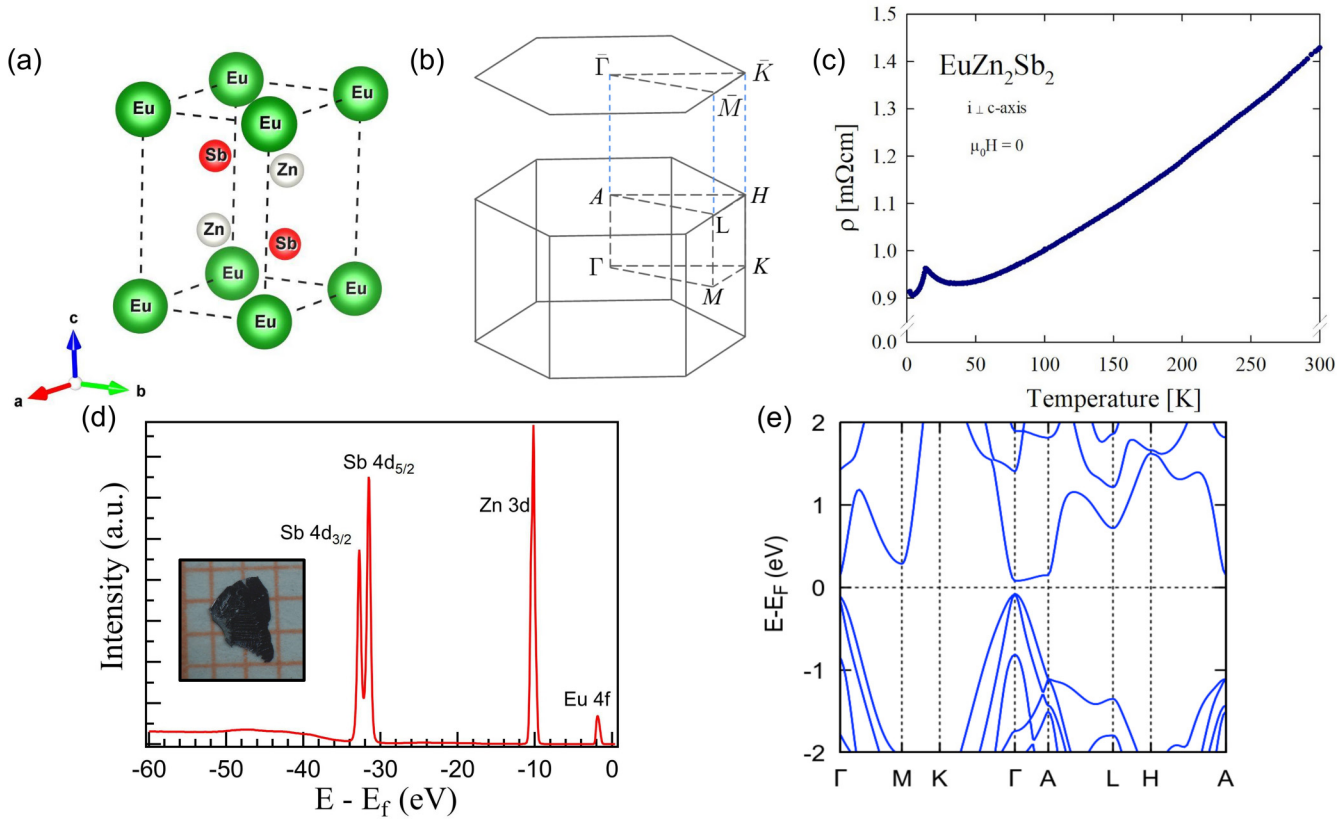

FIG. 1. Crystal structure and sample characterization of $EuZn_2Sb_2$. (a) Crystal structure of $EuZn_2Sb_2$. The green, gray, and red balls identify Eu, Zn, and Sb atoms, respectively. (b) The associated bulk BZ and the surface BZ projected along (001) with high-symmetry points marked. (c) Temperature dependence of the electrical resistivity in zero applied magnetic field measured within the crystallographic *ab* plane. (d) Core-level photoemission spectrum with characteristic peaks of Eu 4*f*, Zn 3*d*, and Sb 4*d* orbitals. A sample photograph is shown in the inset. (e) Nonmagnetic band dispersion calculation along several high-symmetry directions (with taking into account SOC).

interplay between magnetic correlations and spin-orbit coupling induced topology in $EuZn_2Sb_2$ warrants a detailed investigation into the electronic structure of this material. We have carried out angle-resolved photoemission spectroscopy (ARPES) measurements along with parallel density functional theory (DFT) based calculations. We report a direct observation of band spin-degeneracy lifting through an analysis of ARPES line shapes over a range of incident photon energies and sample temperatures in the paramagnetic phase. We observe asymmetric ARPES line shapes that are consistent with the convolution of two distinct band peaks, which persist over a wide temperature range of 15 and 130 K. Our measurements show good agreement with our DFT predictions for the ferromagnetic phase below the Fermi level. Interestingly, our calculations for the spin-split bands are predicted to extend above the Fermi level to generate a single pair of Weyl nodes separated along the k_z direction.

II. METHODS

High-quality $EuZn_2Sb_2$ single crystals were grown by using Zn-Sb flux and characterized using x-ray diffraction and energy-dispersive x-ray spectroscopy [see the Supplemental Material (SM) [34] for growth and characterization details]. High-resolution ARPES measurements were carried out at the Stanford Synchrotron Radiation Laboratory (SSRL) beamline 5-2 and at the Advanced Light Source (ALS) beamline 4.0.3, equipped with Scienta DA30 analyzer and Scienta R8000 electron analyzer, respectively (see SM for further details [34]). All electronic structure calculations were performed within the DFT framework using a plane-wave basis set in the Vienna *ab initio* simulation package (VASP) [35]. The band structures shown in the main text are calculated using the Heyd-Scuseria-Ernzerhof (HSE) functional [36] (see SM for computational details [34]).

III. RESULTS

A. Crystal structure and electronic properties

$EuZn_2Sb_2$ crystallizes in the trigonal space group $P\bar{3}m1$ (No. 164). The unit cell structure consists of alternating Zn_2Sb_2 and Eu layers, as depicted in Fig. 1(a) [37]. A hexagonal bulk BZ is produced by the trigonal lattice [shown in Fig. 1(b)]. This crystal structure has a natural cleave along the (001) plane, which produces the surface-projected BZ shown in relation to the bulk. Previous work on EuX_2Pn_2 samples shows a strong sensitivity of the carrier concentration and Fermi-level position on details of crystal synthesis protocol [38]. Resistivity measurements were performed to check whether the low-energy physics is described by metallic, semimetallic, or semiconducting behavior. Figure 1(c) displays the temperature dependence of the electrical resistivity in single-crystalline $EuZn_2Sb_2$. The sample exhibits metallic behavior with a pronounced anomaly

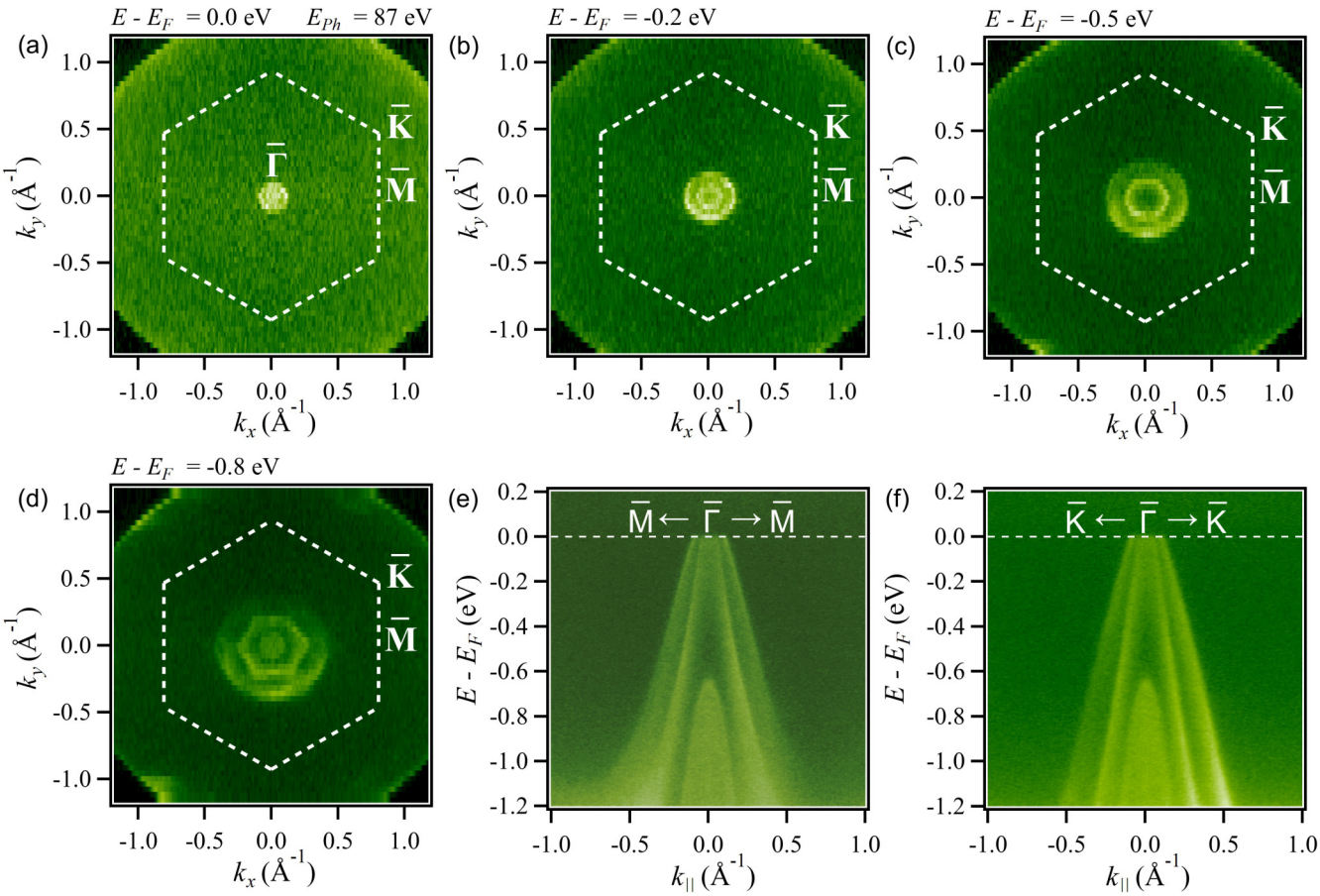

FIG. 2. Constant energy contours (CECs) and dispersion cuts taken with an incident photon energy of 86 eV. (a) The Fermi surface and two CECs at binding energies of (b) 200 meV, (c) 500 meV, and (d) 800 meV. Dispersion cuts along the (e) $\overline{M}$-$\overline{\Gamma}$-$\overline{M}$ and (f) $\overline{K}$-$\overline{\Gamma}$-$\overline{K}$ high-symmetry directions.

at the antiferromagnetic phase transition in the form of a cusplike peak in the resistivity. The Néel temperature, $T_N = 13.3$ K, is close to the value previously reported [37,39]. Notably, the magnitude of $\rho(T)$ is rather large, and the resistivity variation on decreasing temperature is fairly small, which indicates that $EuZn_2Sb_2$ is a bad metal. A negative temperature coefficient above T_N likely arises due to short-range magnetic interactions, while a decrease of the resistivity below T_N is clearly a result of the reduction in electron scattering on the magnetic moments in the ordered state. The short-range magnetic interactions observed above T_N bear a ferromagnetic character, as indicated by the positive value of the paramagnetic Curie temperature derived from the magnetic susceptibility data (see SM [34]). The elemental composition of the sample is corroborated by the core-level photoemission results, which show the presence of atomic peaks at Eu $4f$, Zn $3d$, and Sb $4d$ binding energies [Fig. 1(d)].

In disagreement with the metallic behavior found in electrical resistivity measurements, our nonmagnetic calculations [Fig. 1(e)] predict a direct semiconducting band gap at the Γ point [Fig. 1(e)]. To better understand the valence electronic structure of $EuZn_2Sb_2$, we have performed high-resolution ARPES, the results of which are shown in Figs. 2 and 3. The Fermi surface and several constant energy contours (CECs) are shown in Figs. 2(a)–2(d). The Fermi surface [Fig. 2(a)] consists of two circular hole pockets of small area localized at the $\overline{\Gamma}$ point. The hole nature of the associated bands is evident from the increase in the size of the pocket with increasing binding energy. The dispersion cuts taken along the $\overline{M}$-$\overline{\Gamma}$-$\overline{M}$ [Fig. 2(e)] and $\overline{K}$-$\overline{\Gamma}$-$\overline{K}$ [Fig. 2(f)] directions show that the two hole bands disperse in parallel, where they are joined by the maximum of a third parabolic band at a higher binding energy. The two cuts show a similar dispersion behavior close to the Fermi level, only deviating from one another at higher binding energies.

B. Band splitting induced Weyl semimetal phase

A close inspection of the dispersion cuts reveal the presence of low-intensity parallel dispersing bands, which are not present in the nonmagnetic DFT calculations, as can be seen in Fig. 1(e). To better visualize these split bands, the second derivative (SD) edge detection method was applied to the $\overline{M}$-$\overline{\Gamma}$-$\overline{M}$ dispersion cut [Fig. 3(a)]. The SD figures resolve these features as distinct peaks in the photoemission intensity. In the raw photoemission data, however, these peaks constructively add together to produce an asymmetric momentum distribution curve (MDC) line shape [Figs. 3(b)–3(d)]. We performed a curve fit on the MDC using a Voigt function, which is the convolution of the idealized Lorentzian line shape with Gaussian broadening to account for resolution and temperature effects [40]. Fitted results are shown in Figs. 3(b)–3(d), where each peak is color coded such that

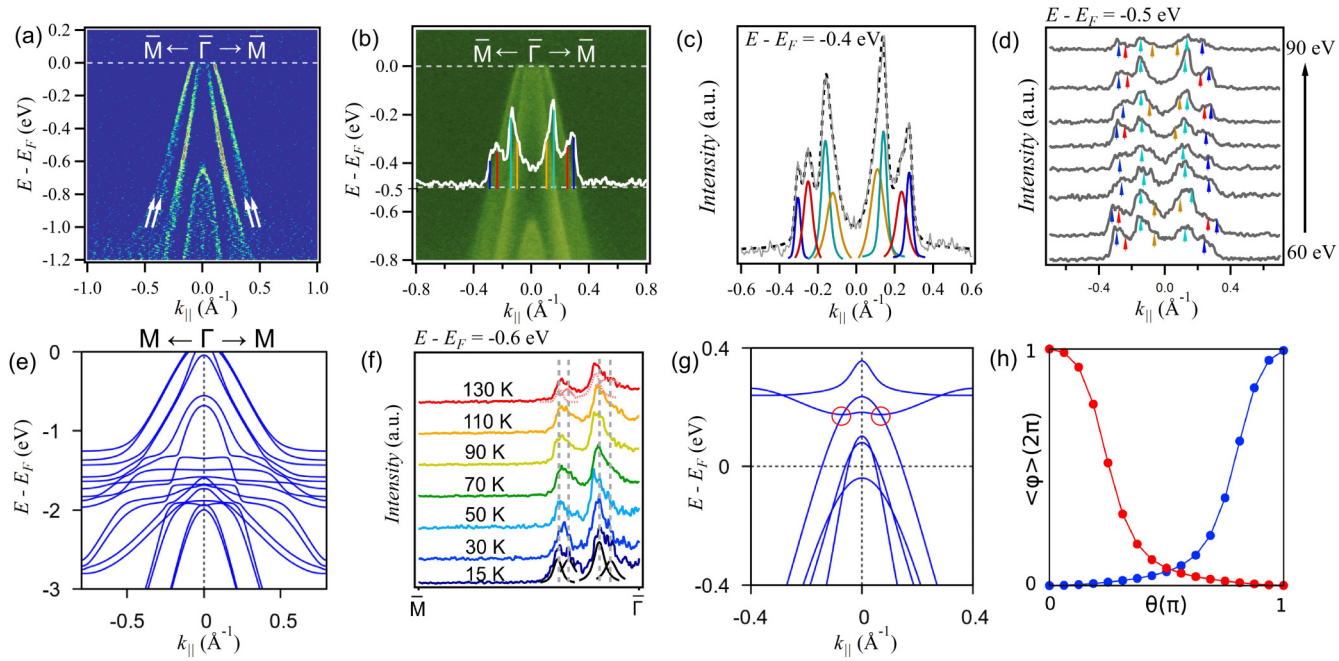

FIG. 3. Observation of spin-split bands in $EuZn_2Sb_2$. SD edge detections applied to the MDCs and displayed for the (a) $\overline{M}$-$\overline{\Gamma}$-$\overline{M}$ direction. (b) MDC at 0.5 eV binding energy integrated over an 8 meV window displayed over the $\overline{M}$-$\overline{\Gamma}$-$\overline{M}$ dispersion cut. Vertical black lines indicate fitted peak positions. (c) Results of Voigt function fit to the MDC at 0.4 eV binding energy. The total fit is given in blue, the individual peaks in green, and the raw MDC in red. (d) MDCs stacked over incident photon energies. Taken along the $\overline{M}$-$\overline{\Gamma}$-$\overline{M}$ direction at a binding energy of 0.5 eV. Eight stacked MDCs for photon energies ranging between 62 and 90 eV corresponding to those in Fig. S2 [34]. Vertical arrows indicate the peak position resulting from the peak fitting for each MDC. The colors indicating the position of the fitted peaks are made consistent between (b)–(d), where blue/red and teal/orange indicate the spin-split pair of the outermost bands and innermost bands, respectively. (e) Result of our ferromagnetic DFT calculations for an out-of-plane magnetization along M-Γ-M. (f) Temperature dependence of the 0.6 eV binding energy MDC along $\overline{M}$-$\overline{\Gamma}$-$\overline{M}$ for temperatures between 15 and 130 K. Fitted peaks are shown at 15 and 130 K. (g) Out-of-plane ferromagnetic calculations above the Fermi level showing the presence of Weyl nodes 180 meV above the Fermi level (circled in red). (h) The chirality of the Weyl points, calculated using the Wannier charge center evolution around a sphere enclosing the gapless points. The red and blue curves are for the two different Weyl points. The Weyl points have chirality ± 1.

the blue/red and teal/orange correspond to the spin-split pairs from the outer and inner bands, respectively. Agreement with the measured MDCs was obtained by including two closely dispersing band pairs, giving an indication of band splitting. The peak positions are indicated for the MDC taken along the $\overline{M}$-$\overline{\Gamma}$-$\overline{M}$ cut at a binding energy of 0.4 eV. The separation of the outer two peaks is about 0.05 ± 0.004 Å^{-1} and about 0.03 ± 0.004 Å^{-1} for the inner bands, as obtained from the difference in the fitted peak positions. The ARPES spectra shown in Figs. 3(a)–3(c) were taken at a photon energy of $h\nu = 86$ eV. To demonstrate the persistence of the band splitting across various photon energies, we have plotted the MDCs for the same $\overline{M}$-$\overline{\Gamma}$-$\overline{M}$ cut for various photon energies ranging from 60 to 90 eV at $E - E_F = -0.5$ eV binding energy, as shown in Fig. 3(d).

Nonmagnetic calculations assign a spin degeneracy to all the bands, including the two outermost hole pockets where spin splitting is observed experimentally (Fig. 3). In accounting for the potential split bands, we repeated the DFT calculation in an out-of-plane ferromagnetic configuration, which produces the pair of nondegenerate parallel dispersive bands [Fig. 3(e)]. The projected size of the band splitting is rather small for the highly dispersive band energies, although the comparison with experimental results establishes the presence of ferromagnetic interactions that result in the splitting of bands. Similar observations in related materials have been attributed to short-range ferromagnetic fluctuations in the paramagnetic phase [17]. Given the presence of slow ferromagnetic correlations ranging from the Néel temperature to over 100 K in $EuZn_2Sb_2$ [20], a similar mechanism can be expected for the observation of the band-splitting feature in our measurements. We repeated measurements of the $\overline{M}$-$\overline{\Gamma}$-$\overline{M}$ dispersion cut over sample temperatures between 15 and 130 K. The temperature variations of the MDCs taken at a binding energy of 0.5 eV are stacked in Fig. 3(f). Weak temperature dependence is seen in the MDC line shapes, which indicates the presence of band splitting up to 130 K, which is consistent with previous reports of the presence of weak ferromagnetic correlations over 100 K [20]. These results show that, even if $EuZn_2Sb_2$ is paramagnetic above 13 K, the presence of weak ferromagnetic domains lifts the spin degeneracy of bands and leads to the observed splitting.

While our nonmagnetic calculations predict a semiconducting gap, our results show two semimetallic hole pockets comprising the Fermi surface. Decreasing the Fermi level by about 180 meV in both the nonmagnetic and ferromagnetic calculations replicates our ARPES results, even though only the ferromagnetic calculations correctly account for the band splitting seen experimentally. Interestingly, our ferromagnetic calculations predict the vanishing of this gap in the

spin-polarized state, which extend to produce a single pair of Weyl nodes along the A-Γ-A direction [Fig. 3(g)]. After accounting for the Fermi-level shift in our calculations, possibly due to hole doping in our samples, the Weyl points are predicted to lie around 180 meV above the Fermi level. We confirm the nontrivial chirality of the Weyl crossings by performing Wannier charge center evolution calculations around a sphere enclosing the gapless point, the results of which are shown in Fig. 3(h). The simultaneous stabilization of the ferromagnetic ground state and electron doping would make $EuZn_2Sb_2$ a candidate minimal Weyl semimetal.

The observation of band splitting in a centrosymmetric and nonmagnetic system may stem from various sources alternate to what has been proposed here. The first possibility is that the observed splitting is surface originated. The spin degeneracy of generic momentum points is in general lifted at the surface due to 3D inversion symmetry breaking [41], which may allow spin-orbit interactions to lift the spin degeneracy. A second explanation for the band splitting is through the influence of crystal defects and domain boundaries. Surface reconstructions could induce modifications in the electronic states near the surface, contributing to the observed band-splitting phenomenon. The influence of surface reconstructions are highly detectable through ARPES measurements through a reduction of the reciprocal space periodicity [42]. However, this scenario contrasts with the data presented in Fig. 2, where no additional periodicity of the bands is observed within the first BZ. Lastly, it is essential to consider the possibility of artifacts caused by k_z broadening, which may arise due to the limited photon escape depth and the presence of multiple photoelectron scattering events [43]. The issue of k_z broadening is an ever-present limitation in VUV ARPES experiments. Such broadening generally leads to an asymmetric line shape in the momentum distribution curves, becoming particularly pronounced at the extreme points of the k_z dispersion. Despite this, we attribute the observed ARPES spectra to the presence of band splitting. The influence of k_z broadening is strongly photon dependent, as modifying the incident photon energy changes the central k_z plane being measured. However, the apparent band splitting does not exhibit a substantial variation with incident photon energy, despite different regions of the valence band being emphasized along k_z.

IV. CONCLUSIONS

Eu-ternary pnictides have been recognized for their simple fermiology, magnetic ordering, as well for their ability to host a nontrivial band topology. Motivated by the recent evidence of local ferromagnetic behavior in the macroscopic paramagnetic phase of $EuZn_2Sb_2$, we report high-resolution ARPES and parallel *ab initio* calculations to unravel how magnetic fluctuations affect the electronic band structure of this material. We adduce evidence that the paramagnetic band spin degeneracy is lifted via an analysis of the MDC line shapes, which is found to display an asymmetric deviation from the expected Voigt function based line shape. This asymmetric line shape is consistent with the spin splitting of electronic states involving slow ferromagnetic fluctuations in the paramagnetic phase, which have been reported in $EuZn_2Sb_2$ even at temperatures greater than 100 K. This is further corroborated by finding weak temperature dependence of the MDC peak splitting up to 130 K and over various incident photon energies. Interestingly, our ferromagnetic calculations, which reproduce our experimental bands, also generate a single pair of Weyl nodes above the Fermi level. Our study identifies $EuZn_2Sb_2$ as a minimal Weyl point candidate and an excellent platform for exploring the interplay between short-range magnetic interactions and electronic band structure.

ACKNOWLEDGMENTS

M.N. acknowledges support from the Air Force Office of Scientific Research MURI Grant No. FA9550-20-1-0322 and the National Science Foundation (NSF) CAREER Award No. DMR-1847962. The work at Northeastern University was supported by the Air Force Office of Scientific Research under Award No. FA9550-20-1-0322 and benefited from the computational resource of Northeastern University's Advanced Scientific Computation Center (ASCC) and the Discovery Cluster. D.K. and T.R. were supported by the National Science Centre (Poland) under Research Grant No. 2021/41/B/ST3/01141. This work utilized resources of the SSRL at the SLAC National Accelerator Laboratory, supported by the U.S. Department of Energy, Office of Science, Office of Basic Energy Sciences under Contract No. DE-AC02-76SF00515. We thank M. Hashimoto and D. Lu for the beamline assistance at SSRL endstation 5-2. This research also used resources of the ALS at the Lawrence Berkeley National Laboratory, a US Department of Energy Office of Science User Facility, under Contract No. DE-AC02-05CH11231. We thank J. Denlinger for beamline assistance at the ALS Beamline 4.0.3.

[1] M. S. Dresselhaus, G. Dresselhaus, and A. Jorio, *Group Theory: Application to the Physics of Condensed Matter* (Springer, Berlin, 2008).
[2] C.-K. Chiu, J. C. Teo, A. P. Schnyder, and S. Ryu, Rev. Mod. Phys. **88**, 035005 (2016).
[3] L. Fu, C. L. Kane, and E. J. Mele, Phys. Rev. Lett. **98**, 106803 (2007).
[4] D. Hsieh, D. Qian, L. Wray, Y. Xia, Y. S. Hor, R. J. Cava, and M. Z. Hasan, Nature (London) **452**, 970 (2008).
[5] Y. Xia, D. Qian, D. Hsieh, L. Wray, A. Pal, H. Lin, A. Bansil, D. Grauer, Y. S. Hor, R. J. Cava, and M. Z. Hasan, Nat. Phys. **5**, 398 (2009).
[6] H. Zhang, C.-X. Liu, X.-L. Qi, X. Dai, Z. Fang, and S.-C. Zhang, Nat. Phys. **5**, 438 (2009).
[7] M. Z. Hasan and C. L. Kane, Rev. Mod. Phys. **82**, 3045 (2010).
[8] X.-L. Qi and S.-C. Zhang, Rev. Mod. Phys. **83**, 1057 (2011).
[9] A. Bansil, H. Lin, and T. Das, Rev. Mod. Phys. **88**, 021004 (2016).

[10] S. M. Young, S. Zaheer, J. C. Teo, C. L. Kane, E. J. Mele, and A. M. Rappe, Phys. Rev. Lett. **108**, 140405 (2012).
[11] Z. Wang, Y. Sun, X.-Q. Chen, C. Franchini, G. Xu, H. Weng, X. Dai, and Z. Fang, Phys. Rev. B **85**, 195320 (2012).
[12] M. Neupane, S.-Y. Xu, R. Sankar, N. Alidoust, G. Bian, C. Liu, I. Belopolski, T.-R. Chang, H.-T. Jeng, H. Lin, A. Bansil, F. Chou, and M. Z. Hasan, Nat. Commun. **5**, 3786 (2014).
[13] N. P. Armitage, E. J. Mele, and A. Vishwanath, Rev. Mod. Phys. **90**, 015001 (2018).
[14] Y. Tokura, K. Yasuda, and A. Tsukazaki, Nat. Rev. Phys. **1**, 126 (2019).
[15] B. Yan and C. Felser, Annu. Rev. Condens. Matter Phys. **8**, 337 (2017).
[16] J. Sokoloff, J. Phys. F: Met. Phys. **5**, 528 (1975).
[17] J.-Z. Ma, S. M. Nie, C. J. Yi, J. Jandke, T. Shang, M. Y. Yao, M. Naamneh, L. Q. Yan, Y. Sun, A. Chikina, V. N. Strocov, M. Medarde, M. Song, Y.-M. Xiong, G. Xu, W. Wulfhekel, J. Mesot, M. Reticcioli, C. Franchini, C. Mudry *et al.*, Sci. Adv. **5**, eaaw4718 (2019).
[18] Y. Xu, L. Das, J. Z. Ma, C. J. Yi, S. M. Nie, Y. G. Shi, A. Tiwari, S. S. Tsirkin, T. Neupert, M. Medarde, M. Shi, J. Chang, and T. Shang, Phys. Rev. Lett. **126**, 076602 (2021).
[19] E. Yi, D. F. Zheng, F. Pan, H. Zhang, B. Wang, B. Chen, D. Wu, H. Liang, Z. X. Mei, H. Wu, S. A. Yang, P. Cheng, M. Wang, and B. Shen, Phys. Rev. B **107**, 035142 (2023).
[20] Y. Goryunov, V. Fritsch, H. v. Löhneysen, and A. Nateprov, J. Phys.: Conf. Ser. **391**, 012015 (2012).
[21] Y. Goryunov and A. Nateprov, JPS Conf. Proc. **3**, 011026 (2014).
[22] J.-R. Soh, E. Schierle, D.-Y. Yan, H. Su, D. Prabhakaran, E. Weschke, Y.-F. Guo, Y.-G. Shi, and A. T. Boothroyd, Phys. Rev. B **102**, 014408 (2020).
[23] L.-L. Wang, N. H. Jo, B. Kuthanazhi, Y. Wu, R. J. McQueeney, A. Kaminski, and P. C. Canfield, Phys. Rev. B **99**, 245147 (2019).
[24] Y. Xu, Z. Song, Z. Wang, H. Weng, and X. Dai, Phys. Rev. Lett. **122**, 256402 (2019).
[25] T. Sato, Z. Wang, D. Takane, S. Souma, C. Cui, Y. Li, K. Nakayama, T. Kawakami, Y. Kubota, C. Cacho, T. K. Kim, A. Arab, V. N. Strocov, Y. Yao, and T. Takahashi, Phys. Rev. Res. **2**, 033342 (2020).
[26] S. Regmi, M. M. Hosen, B. Ghosh, B. Singh, G. Dhakal, C. Sims, B. Wang, F. Kabir, K. Dimitri, Y. Liu, A. Agarwal, H. Lin, D. Kaczorowski, A. Bansil, and M. Neupane, Phys. Rev. B **102**, 165153 (2020).
[27] H. Su, B. Gong, W. Shi, H. Yang, H. Wang, W. Xia, Z. Yu, P.-J. Guo, J. Wang, L. Ding, L. Xu, X. Li, X. Wang, Z. Zou, N. Yu, Z. Zhu, Y. Chen, Z. Liu, K. Liu, G. Li *et al.*, APL Mater. **8**, 011109 (2020).
[28] K. Singh, O. Pavlosiuk, S. Dan, D. Kaczorowski, and P. Wiśniewski, Phys. Rev. B **109**, 125107 (2024).
[29] S. X. M. Riberolles, T. V. Trevisan, B. Kuthanazhi, T. W. Heitmann, F. Ye, D. C. Johnston, S. L. Budko, D. H. Ryan, P. C. Canfield, A. Kreyssig, A. Vishwanath, R. J. McQueeney, L. L. Wang, P. P. Orth, and B. G. Ueland, Nat. Commun. **12**, 999 (2021).
[30] M. Sprague, A. P. Sakhya, S. Regmi, M. I. Mondal, I. B. Elius, N. Valadez, K. Booth, T. Romanova, A. Ptok, D. Kaczorowski, and M. Neupane, Phys. Rev. Mater. **8**, 054411 (2024).
[31] X. Gui, I. Pletikosic, H. Cao, H.-J. Tien, X. Xu, R. Zhong, G. Wang, T.-R. Chang, S. Jia, T. Valla, W. Xie, and R. J. Cava, ACS Cent. Sci. **5**, 900 (2019).
[32] H. Li, S.-Y. Gao, S.-F. Duan, Y.-F. Xu, K.-J. Zhu, S.-J. Tian, J.-C. Gao, W.-H. Fan, Z.-C. Rao, J.-R. Huang, J.-J. Li, D.-Y. Yan, Z.-T. Liu, W.-L. Liu, Y.-B. Huang, Y.-L. Li, Y. Liu, G.-B. Zhang, P. Zhang, T. Kondo *et al.*, Phys. Rev. X **9**, 041039 (2019).
[33] N. H. Jo, B. Kuthanazhi, Y. Wu, E. Timmons, T.-H. Kim, L. Zhou, L.-L. Wang, B. G. Ueland, A. Palasyuk, D. H. Ryan, R. J. McQueeney, K. Lee, B. Schrunk, A. A. Burkov, R. Prozorov, S. L. Bud'ko, A. Kaminski, and P. C. Canfield, Phys. Rev. B **101**, 140402(R) (2020).
[34] See Supplemental Material at http://link.aps.org/supplemental/10.1103/PhysRevB.110.045130 for supplemental results. References for our transport [37,39,44], calculations [35,36,45,46], and MDC analyses [40,47] are also provided for further information.
[35] G. Kresse and J. Furthmüller, Phys. Rev. B **54**, 11169 (1996).
[36] G. Kresse and D. Joubert, Phys. Rev. B **59**, 1758 (1999).
[37] F. Weber, A. Cosceev, S. Drobnik, A. Faisst, K. Grube, A. Nateprov, C. Pfleiderer, M. Uhlarz, and H. v. Löhneysen, Phys. Rev. B **73**, 014427 (2006).
[38] D. Santos-Cottin, I. Mohelský, J. Wyzula, F. L. Mardelé, I. Kapon, S. Nasrallah, N. Barišić, I. Živković, J. R. Soh, F. Guo *et al.*, Phys. Rev. Lett. **131**, 186704 (2023).
[39] H. Zhang, J.-T. Zhao, Y. Grin, X.-J. Wang, M.-B. Tang, Z.-Y. Man, H.-H. Chen, and X.-X. Yang, J. Chem. Phys. **129**, 164713 (2008).
[40] G. Levy, W. Nettke, B. M. Ludbrook, C. N. Veenstra, and A. Damascelli, Phys. Rev. B **90**, 045150 (2014).
[41] A. Manchon, H. C. Koo, J. Nitta, S. M. Frolov, and R. A. Duine, Nat. Mater. **14**, 871 (2015).
[42] S. Liu, W. Xia, K. Huang, D. Pei, T. Deng, A. J. Liang, J. Jiang, H. F. Yang, J. Zhang, H. J. Zheng, Y. J. Chen, L. X. Yang, Y. F. Guo, M. X. Wang, Z. K. Liu, and Y. L. Chen, Phys. Rev. B **103**, 115127 (2021).
[43] V. N. Strocov, J. Electron Spectrosc. Relat. Phenom. **130**, 65 (2003)
[44] A. F. May, M. A. McGuire, J. Ma, O. Delaire, A. Huq, and R. Custelcean, J. Appl. Phys. **111**, 033708 (2012).
[45] J. Heyd, G. E. Scuseria, and M. Ernzerhof, J. Chem. Phys. **118**, 8207 (2003).
[46] J. Heyd, J. E. Peralta, G. E. Scuseria, and R. L. Martin, J. Chem. Phys. **123**, 174101 (2005).
[47] A. Damascelli, Z. Hussain, and Z.-X. Shen, Rev. Mod. Phys. **75**, 473 (2003).